Biomaterials Advances 161 (2024) 213889

Contents lists available at ScienceDirect

Biomaterials Advances

journal homepage: www.journals.elsevier.com/materials-science-and-engineering-c

Novel nano-in-micro fabrication technique of diclofenac nanoparticles loaded microneedle patches for localised and systemic drug delivery

Mingshan Li, Lalitkumar K. Vora *, Ke Peng, Akmal H.B. Sabri, Nuoya Qin, Marco Abbate, Alejandro J. Paredes, Helen O. McCarthy, Ryan F. Donnelly *

School of Pharmacy, Medical Biology Centre, Queen's University Belfast, 97 Lisburn Road, Belfast BT9 7BL, Northern Ireland, United Kingdom

ARTICLE INFO

Keywords:
Nano-in-micro
Pain management
Diclofenac
Nanoparticle
Microneedle
Anti-inflammation
Sustained delivery
Transdermal delivery
Localised delivery

ABSTRACT

Diclofenac, a nonsteroidal anti-inflammatory drug, is commonly prescribed for managing osteoarthritis, rheumatoid arthritis, and post-surgical pain. However, oral administration of diclofenac often leads to adverse effects. This study introduces an innovative nano-in-micro approach to create diclofenac nanoparticle-loaded microneedle patches aimed at localised, sustained pain relief, circumventing the drawbacks of oral delivery. The nanoparticles were produced *via* wet-milling, achieving an average size of 200 nm, and then incorporated into microneedle patches. These patches showed improved skin penetration in *ex vivo* tests using Franz-cell setups compared to traditional diclofenac formulations. *In vivo* tests on rats revealed that the nanoparticle-loaded microneedle patches allowed for quick drug uptake and prolonged release, maintaining drug levels in tissues for up to 72 h. With a systemic bioavailability of 57 %, these patches prove to be an effective means of transdermal drug delivery. This study highlights the potential of this novel microneedle delivery system in enhancing the treatment of chronic pain with reduced systemic side effects.

1. Introduction

Osteoarthritis (OA) is a prevalent condition that primarily affects the elderly population and results in various symptoms, including pain and joint dysfunction [1,2]. It poses a considerable public health challenge globally and is often associated with obesity and aging [3]. Several nonpharmacological and pharmacological interventions are currently available to alleviate pain and improve the patient's quality of life [4,5]. Nonpharmacological therapies include exercise and weight management, while pharmacologic treatment options include oral and topical administration of nonsteroidal anti-inflammatory drugs (NSAIDs) and intra-articular injection of corticosteroids according to the osteoarthritis research society international (OARSI) guidelines [6]. Microneedles (MN) have emerged as a promising technology for drug delivery, enabling efficient drug delivery that is painless and minimally invasive, making them an attractive alternative to traditional injections or topical formulations for both localised and systemic delivery in the treatment of OA [7,8].

Diclofenac (DCF) is one of the most studied NSAIDs in the treatment of OA [10]. Several commercial products have been practically applied including topical gel, topical solution and topical plaster. To date, the increasing number of topical DCF products introduced to the market (Olfen®, Voltaren®, Flector® *etc.*) is an indication of growing appeal of transdermal delivery of DCF. Nevertheless, delivering DCF *via* the transdermal route suffers several challenges, as the drug is intrinsically hydrophobic (log P: 4.51), which limits the amount of the drug that can be delivered across the skin through topical formulations [11]. Owing to these drawbacks, diclofenac sodium (DS), a soluble salt form, is utilized in various formulations, including topical applications, to enhance solubility and skin permeability.

In recent years, the convergence of nanoparticles and MN patches has emerged as a breakthrough in drug delivery [12–18]. This innovative approach addresses challenges such as the hydrophobicity and poor permeability of drugs, creating a sophisticated composite pharmaceutical platform that is capable of delivering drugs in a localised and extended manner for the management of disease [19–21].

Despite the growing interest in the topical delivery of DCF among scientists and the pharmaceutical industry, research into the combination of DCF nanoparticles (DCF-NPs) and MN systems currently remains limited [22]. Pireddu *et al.* conducted a study in which a DERMA-Q roller was used to pretreat the skin before applying DCF nanosuspensions stabilised with poloxamer-188 and Tween-80 to enhance

* Corresponding authors at: School of Pharmacy, Queens University Belfast, United Kingdom.
E-mail addresses: l.vora@qub.ac.uk (L.K. Vora), R.Donnelly@qub.ac.uk (R.F. Donnelly).

https://doi.org/10.1016/j.bioadv.2024.213889
Received 5 January 2024; Received in revised form 3 May 2024; Accepted 7 May 2024
Available online 9 May 2024

delivery [23]. The current study fabricated DCF-NPs with satisfactory stability and a small particle size. Our MN fabrication method leverages the "nano-in-micro" strategy to encapsulate these nanoparticles within the tips of MNs, utilizing preformed PLA baseplates for improved precision and reliability (as illustrated in Fig. 1). The integration of these preformed baseplates streamlines the fabrication process, significantly reduces preparation time, and ensures consistent drug delivery and structural integrity across the MN arrays. This study also includes a comprehensive investigation to compare MNs loaded with DCF, DCF-NP and DS, with commercial Voltarol® gel as well as oral DCF administration. This investigation provides valuable insights into the transdermal delivery of DCF. It is hoped that the pharmaceutical system developed in this study offers a potential solution for delivering DCF both locally and systemically in a sustained and patient-friendly manner, thereby improving the management and treatment of OA.

2. Materials and methods

2.1. Materials and apparatus

DCF and DS were purchased from Tokyo Chemical Industry (Oxford, UK). Poly(vinyl alcohol) (PVA, MW 9000–10,000) was purchased from Sigma–Aldrich (St. Louis, MO, U.S.). Plasdone™ K-29/32 (Povidone, PVP, 60 kDa) was obtained from Ashland (Wilmington, Delaware, U.S.). Phosphate buffered saline (PBS) tablets (pH 7.3–7.5) and Tween® 80 (reagent grade) were purchased from VWR Life Science (Basingstoke, UK). Acetonitrile (HPLC grade) and methanol (HPLC grade) were purchased from Sigma–Aldrich (St. Louis, MO, U.S.). All other chemicals were of analytical reagent grade. Heparin sodium flushing solution, 100 I.U./mL (200 units in 2 mL) was obtained from Wockhardt (Wrexham, UK). The depilatory cream Veet® was purchased from Reckitt (Slough, UK). Stillborn piglets were obtained from a local farm immediately after birth and stored at −20 °C until further use.

Yttria-stabilised zirconia beads were purchased from Chemco Advance Material (Suzhou, China). The magnetic stirring plate was a Magnetic Stirrer IKA® RCT basic (Staufen, Germany). Particle analysis was performed by a NanoBrook Omni™ Particle size and zeta potential analyser (Brookhaven Instruments, Holtsville, NY, U.S.). The HPLC was an Agilent 1260 Infinity II LC system (Agilent Technologies UK Ltd., Stockport, UK). The analysis was accomplished using an ODS-3 analytical column (250 mm × 4.6 mm internal diameter, 5 μm packing, Phenomenex, Cheshire, UK). Lyophilisation was achieved by a VirTis Advantage freeze-dryer (SP Industries Inc., Warminster, PA, U.S.). A SpeedMixer™ (DAC 150.1 FVZ—K, Synergy Devices Ltd., High Wycombe, UK) was used in the MN formulation preparation. The pressure chamber used in the experiments was a pressure tank (Protima®, TUV Rheinland, Pittsford, NY, U.S.). The porcine skins and Parafilm M® layers were observed by optical coherence tomography (OCT, EX1301,

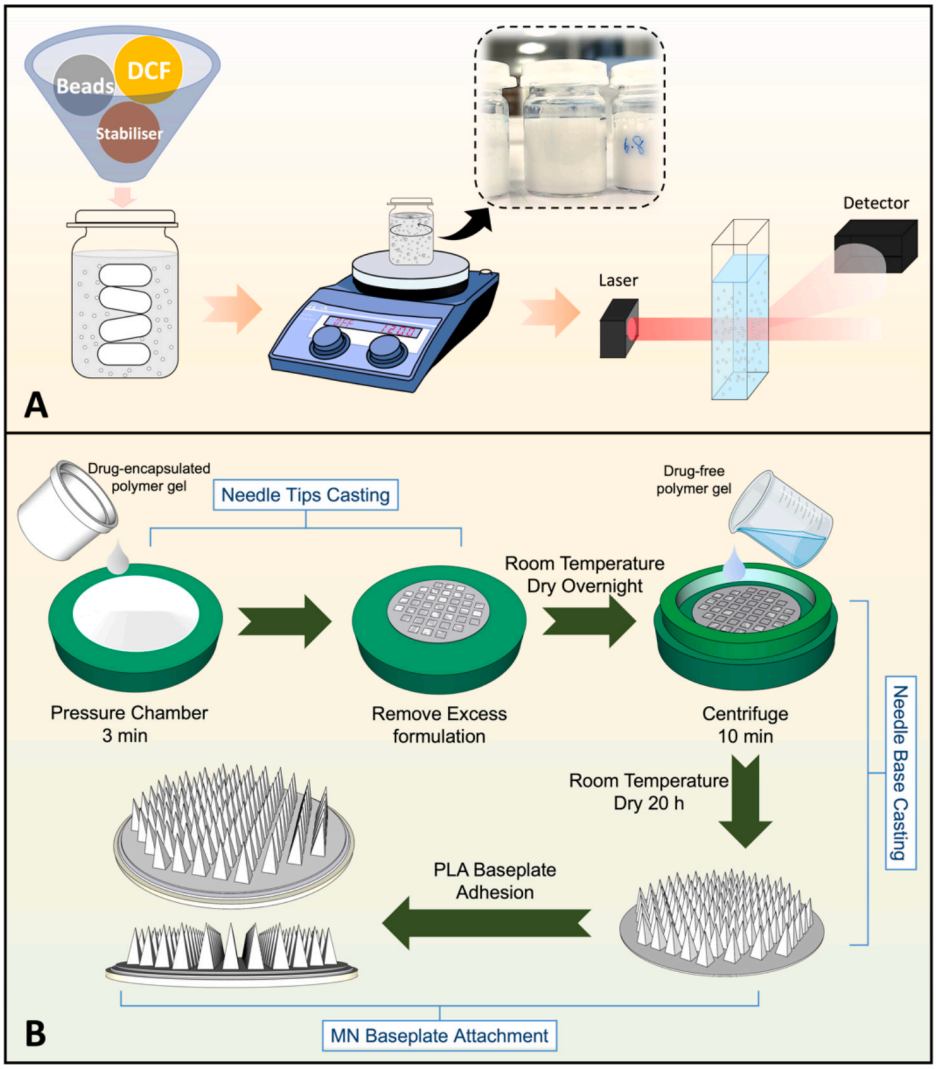

Fig. 1. (A) Fabrication of DCF nanosuspensions using a wet bead milling approach. (B) Manufacture of trilayer MN patches loaded with drug.

Michelson Diagnostics Ltd., Kent, UK) and light microscopy (LEICA EZ4 W, Wetzlar, Germany). The Glue dots® used in the MN manufacture process were purchased from Daler-Rowney Ltd. (Bracknell, UK). MN patches were inserted using a TA. XT plus Texture Analyser™ (Stable Microsystems, Haslemere, UK). A TissueLyser™ LT (QIAGEN, Germantown, USA) was used for tissue disruption. The Microfoam™ and Tegaderm™ were purchased from 3 M (St Paul, Minnesota, USA).

2.2. Fabrication of DCF-NPs

DCF-NPs were prepared using the wet bead milling method illustrated in Fig. 1-A [24,25]. A glass vial containing 200 mg of DCF, 2 mL of zirconia beads (0.1 mm), four magnetic stirring bars (12 × 6 mm), and 5 mL of aqueous stabiliser solution (2 % *w/v*, PVA MW 9–10 K: PVP MW 58 K = 2:3) was placed on a magnetic stirring plate. The stirring speed was set to 1200 rpm. Nanoparticle sizes were measured using a particle sizer at 3 h, 6 h and 20 h. The DCF nanosuspensions were then filtered through a 0.05 mm sieve and subjected to freeze-drying. The protocol of freeze-drying is described in Supplementary S.3.

2.3. In vitro drug dissolution

The *in vitro* drug dissolutions of DCF-P and DCF-NPs were assessed using the dialysis method. The drug powders were dispersed in 2 mL of PBS with 2 % Tween-80 and added to dialysis membranes (12–14 kDa molecular weight cut-off). The membranes were sealed, placed in bottles with release media (200 mL of PBS with 2 % Tween-80), and incubated at 37 °C and 80 rpm. Samples were collected at various time points, and fresh blank release media was added. The samples were purified by high-speed centrifugation (16,163 ×*g*, 15 min) and quantified using HPLC (HPLC method: Supplementary S.4, Table 2). DDSolver, a Microsoft Excel add-in tool for drug dissolution analysis, was used to examine the *in vitro* dissolution kinetics.

2.4. Manufacture and characterisation of drug-loaded trilayer MNs

The MN patches were produced using a mould-casting method (Fig. 1-B) [26–28]. To prepare the casting formulations, freeze-dried DCF-NPs were mixed with deionised water, DCF-P was mixed with polymer aqueous gel (35 %, PVA MW 9–10 K: PVP MW 58 K = 3:4), and formulations were homogenised at a rate of 3500 rpm for 5 min using the SpeedMixer™. The casting formulation contained 27 % drug, 13 % polymer, and 60 % water.

The casting formulation was dispensed onto the mould surface and transferred to a pressure chamber. It was then pressed at 60 psi for 3 min to fill the mould cavities. After removing the excess formulation and drying overnight, the tips were formed in the cavities. A blank polymer layer was cast using 0.27 g of aqueous polymer gel (35 %, PVA MW 9–10 K: PVP MW 58 K = 3:4), centrifuged at 2205 ×*g* for 10 min, and dried [29]. The 3D-printed baseplate was attached to the blank polymer layer with a Glue dot®, and the MN patch was detached from the mould [30].

Different silicone moulds were employed for casting the MNs loaded with DCF-NPs to evaluate drug loading and insertion of MN patches. These included a 600-needle array mould (600-MN mould, pyramidal needles), a 14 × 14 array mould (conical needles), a 19 × 19 array mould (pyramidal needles), and a 16 × 16 array mould (pyramidal needles with column shaft). The detailed dimensions of the different moulds are shown in Fig. 3.

The mechanical properties of drug-loaded MN patches were evaluated using the Texture Analyser™, following the settings described in a previous study for pressing force, moving rate, and holding time [30]. To assess the insertion depth, the MN patches were inserted into folded Parafilm M® sheets (eight layers, approximately 1 mm thick), and the needle tips were compressed against an aluminium block to measure the needle height reduction.

The surface morphology and shape of the DCF and DCF-NP loaded MN arrays were analysed using a Keyence VHX-700F Digital Microscope (Keyence, Osaka, Japan) and a scanning electron microscope (SEM)—specifically, the FEI Quanta FEG 250 Environmental SEM equipped with an Oxford Ex-ACT detector. These SEM analyses were conducted at acceleration voltages ranging from 10 to 20 kV, under a high vacuum condition of 8×10^{-5} mbar, using standard SEM carbon tape for background.

2.5. Ex vivo skin insertion, deposition and permeation of drug-loaded MN patches

The excised full-thickness neonatal porcine skins were pretreated by shaving and equilibrating in PBS for 30 min. Manual insertion of MN patches into the skin using the thumb was followed by a 30-s application. The porcine skins were then observed using an OCT microscope.

To assess *ex vivo* drug deposition, an "oven model" was employed [31,32]. MN-inserted full-thickness neonatal porcine skin samples were placed on PBS-saturated tissue paper to maintain moisture during the 24-h experiment. After incubation at 37 °C, the skin samples were collected and carefully cleaned to remove excess formulation and gel residue. The drug depots were extracted using methanol and quantified using HPLC.

The permeation of drugs through the skin was investigated using a Franz-cell diffusion model. The receptor chamber was filled with pre-heated PBS (12 mL), and the full-thickness porcine skin was positioned between the receptor and donor chamber. The MN patch was manually inserted into the porcine skin, and a 12 g metal weight was applied to maintain its stability. Samples were collected from the sampling port, and the receptor chamber was replenished with fresh release media PBS.

2.6. In vivo pharmacokinetics and drug distribution

These *in vivo* studies were conducted according to the policy of the Federation of European Laboratory Animal Science Associations and the European Convention for the Protection of Vertebrate Animals Used for Experimental and Other Scientific Purposes, following the principles of the 3Rs (replacement, reduction, and refinement). The Committee of Biological Service Unit, Queen's University Belfast, granted approval for the animal experiments conducted in this study under Project Licence PPL 2903 and Personal Licences PIL 1892, PIL 2056 and PIL 2154. For this study, female Sprague-Dawley rats, aged 9–10 weeks at the start of the experiment, were sourced from Charles River Laboratories in Harlow, UK. To study the pharmacokinetics and biodistribution of DCF-NPs in rats, two administration routes were employed: oral gavage and MN patches. Female Sprague–Dawley rats were acclimated for seven days prior to the experiment. The rats were divided into two groups: (a) 8 rats with a mean body weight of 231.88 ± 19.59 g (mean ± SD, $n = 8$) received DCF-NPs orally at a dose of 15 mg/kg (equivalent to 10 mg/kg DCF). DCF-NPs (3.5 mg/rat, equivalent to 2.3 mg DCF) were reconstituted in 1 mL of sterile water and sonicated to achieve a uniform formulation with a concentration of 3.5 mg/mL; (b) 8 rats with a mean body weight of 221.5 ± 20.04 g (mean ± SD, $n = 8$) were administered two patches of DCF-NP MNs at a dose of 30 mg/kg.

For the MN application cohort, the dorsal hair of the rats was shaved with electric hair clippers, and the remaining hair was removed with depilatory cream (Veet®). Hair removal was performed the day before MN application to allow for recovery of skin barrier function [33]. On the day of the experiment, DCF-NP MNs were attached to Microfoam™ and applied to the back of the rats. Tegaderm™ films were then adhered on top of Microfoam™ with MNs, after which the applied MNs were wrapped using kinesiology tape to prevent them from moving or falling off due to gnawing or daily activity of rats.

Blood samples were collected into heparinised tubes through tail vein bleeding at predetermined time intervals, *i.e.*, 1 h, 2 h, 4 h, 24 h, 30 h, 48 h and 72 h. Additionally, four rats from each cohort were culled at

the 24-h time point to examine the distribution of DCF in the skins (at the application site), muscles (beneath the application site) and legs. The paws were severed from the legs, and the attached skin and muscles were carefully removed using tweezers. The remaining paws were rapidly frozen using liquid nitrogen and then fragmented with a hammer. The skins and muscles collected from the dorsal area of the rats were cut into small pieces using scissors in an Eppendorf tube. High-throughput tissue disruption of the rat tissues was performed using the TissueLyser™ LT at a speed of 3000 oscillations/min. The drug was extracted using methanol and quantified using LC–MS.

PKSolver, a Microsoft Excel add-in tool for pharmacokinetics data analysis, was used to examine the *in vivo* pharmacokinetics of DCF delivered orally and *via* MNs [34]. The area under the curve (AUC) of the drug concentration-time curve was calculated using Prism software.

The relative systemic bioavailability (F) of different administrations was calculated using Eq. (1) below:

$$F_{(DCF-NP\ MN)relative} = \frac{AUC_{DCF-NP\ MN} \times dose_{oral}}{AUC_{oral} \times dose_{DCF-NP\ MN}} \quad (1)$$

The delivery efficiency was calculated using Eq. (2) below:

$$Efficiency_{(DCF-NP\ MN)} = F_{oral} \times \frac{AUC_{DCF-NP\ MN} \times dose_{oral}}{AUC_{oral} \times dose_{DCF-NP\ MN}} \quad (2)$$

2.7. Statistical analysis

The data are presented as the means ± SDs, and statistical analysis was performed using Student's *t*-test and analysis of variance (ANOVA). One-way ANOVA was employed for analysing a single independent variable, and Two-way ANOVA was utilized for analysing two independent variables. The statistical analysis was performed using Prism software, with the significance level was set at $p = 0.05$.

3. Results and discussion

MN patches were developed to intradermally deliver DCF by loading the nanoparticulate DCF into micron size MNs. These patches act as a self-implanting drug reservoir placed intradermally, enabling regional and sustained drug release while minimizing systemic side effects. When applied to the skin, the MN painlessly penetrates the epidermis, forming microscopic aqueous channels to deposit the DCF-NPs that allow drugs to diffuse into the dermal microcirculation.

3.1. Fabrication of DCF-NPs and evaluation of in vitro release

3.1.1. Particle size reduction

DCF-NPs were produced through a wet-milling technique, and their size was accurately measured using a particle sizing instrument. Fig. 2-A illustrates the inverse relationship between milling time and the particle size as well as polydispersity index (PDI) of DCF nanosuspensions. As shown in Fig. 2-A, the particle size was significantly reduced by continuous milling from 111.2 μm initially to 211.2 ± 11.5 nm after 20 h of milling ($p < 0.0001$). Initially, after three hours of milling, a significant reduction in particle size was observed, from 111.2 ± 18.7 μm to 297.4 ± 32.7 nm ($p < 0.0001$). Further milling led to additional reductions in particle size, with sizes of 254.3 ± 23.9 nm and 211.2 ± 11.5 nm achieved after 6 and 20 h, respectively. PDI values also decreased significantly with increasing milling time ($p = 0.006$). The smaller PDI values reflect a more uniform particle distribution and may contribute to improved particle stability. Based on these results, a milling duration of 20 h was chosen for subsequent DCF nanosuspension preparation. Particle size and PDI values are included in Supplementary S.1. The fabricated DCF nanosuspensions exhibited stability in liquid form for up to three weeks when stored at 4 °C ($p = 0.3695$). The stability study is included in Supplementary S.2.

SEM images of DCF and DCF-NP loaded MN tips are shown in Fig. 2-B. The comparison of the two types of MN tips showed that the edges of the MN tips loaded with DCF-NPs were smoother than those loaded with DCF, with the absence of large crystals in the former.

3.1.2. Saturation solubility study and in vitro release

To investigate the differences in saturation solubility and *in vitro* dissolution profiles between DCF and DCF-NPs, comprehensive studies were conducted. The measured saturation solubilities in PBS at 37 °C over 24 h for DCF and DCF-NPs were 1.08 ± 0.04 mg/mL and 1.36 ± 0.05 mg/mL, respectively (means ± SDs, $n = 3$). Notably, DCF-NPs exhibited a 25 % increase in saturation solubility compared to DCF-P ($p = 0.0018$). The increase in saturation solubility of DCF-NPs was expected according to the Ostwald-Freundlich equation (Eq. (3)), where the saturation solubility (Cs) increases with decreasing particle size, and this increase can be seen when the particle size is below 1 μm [35].

$$log\frac{C_s}{C_\infty} = \frac{2\sigma V}{2.303RT\rho r} \quad (3)$$

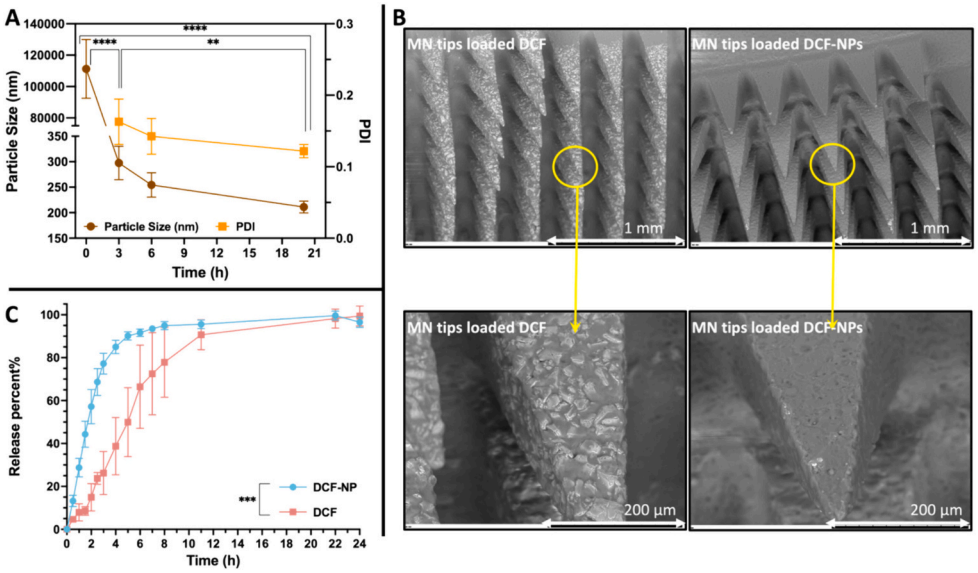

Fig. 2. (A) Variation in DCF particle size and PDI with milling time (means ± SDs, $n = 10$). (B) SEM observation of MN tips loaded with DCF/DCF-NP. (C) *In vitro* release of DCF coarse powder and DCF-NP (means ± SDs, $n = 3$).

where C_s = solubility, C_∞ = solubility of the solid consisting of large particles, σ = interfacial tension substance, V = molar volume of the particle material, R = gas constant, T = absolute temperature, ρ = density of the solid, r = radius.

Fig. 2-C illustrates that DCF-NPs dissolve faster than diclofenac powder (DCF-P), with DCF-NPs releasing half the drug in just 1.7 h and 80 % in 3.4 h, compared to 4.1 h and 6.7 h for DCF-P. This quicker dissolution is likely due to the smaller particle size of the NPs, which increases the surface area available to interact with solvents [39]. The more consistent and smoother release of DCF-NPs suggests they could improve how effectively the drug passes through the skin when used in MN patches. Essentially, DCF-NPs are better suited for MN patches because they could enhance the drug's availability through the transdermal route when applied to the skin.

3.2. Freeze-drying of DCF nanosuspensions

To maximise the drug concentration within the casting gel and therefore increasing the drug loading, freeze-drying was employed to remove excess water from DCF nanosuspensions. Prior to MN casting, the freeze-dried DCF-NPs were reconstituted with a minimal quantity of water, resulting in a concentrated drug-polymer aqueous gel.

Freeze-drying is commonly used in the pharmaceutical industry for the preservation of active substances, such as proteins, liposomes and drug NPs, since the samples can then be stored and transported in a stable dry state at room temperature [36]. The most common freeze-drying protective agents are sugars (glucose, sucrose, trehalose, *etc.*), polymers (PVP, poly(ethylene glycol), dextran, *etc.*) and polyols (sorbitol, mannitol, *etc.*) [38,39].

Here, PVP (10 K, 58 K), PVA (9–10 K) and their mixture were applied in the freeze-drying process to protect the stability of the DCF-NPs. The results are presented in Table 1.

The particle size before freeze-drying was 343.46 ± 5.81 nm with a PDI value of 0.210 ± 0.018 (means ± SDs, n = 3). As seen from the results, the individual application of PVP 10 K failed to stabilise the DCF-NPs during the freeze-drying process, manifesting in the macroscopic particles observed during reconstitution. In contrast, the application of PVA 9–10 K and its mixture with PVP 58 K stabilised the DCF-NPs more effectively, thus allowing them to be successfully reconstituted after freeze-drying and to obtain nano sizes comparable to the initial size. The polymer-drug ratio required to stabilise the DCF-NPs was then evaluated, and the results are shown in Supplementary S. Table 2.

From Table 1 and S. Table 2, It was observed that polymer: drug ratios of 1:6 and 1:3 failed to stabilise the DCF-NPs, whereas ratios of 1:1, 2:3 and 1:2 successfully protected the DCF-NPs, allowing for their reconstitution after freeze-drying. For optimal drug loading in the MNs, a polymer:drug ratio of 1:2 was selected for the fabrication of DCF-NPs. The parameters of the DCF-NPs before and after freeze-drying are presented in Table 2.

3.3. Manufacture of different drug-loaded MNs and evaluation

The ability of MN patches to effectively deliver drugs is considerably controlled by their physical and mechanical properties, including needle strength, insertion depth, and drug loading capacity [40]. These essential properties are determined not only by the materials selected for MN fabrication but also by the design of the MN patches. MN design parameters, including needle height, base width, spacing, and shape, play critical roles in influencing these characteristics [33,41]. According to the existing literature, conical and pyramidal shapes are the most frequently employed geometries in MN design [42]. In pursuit of identifying an optimised MN system, four distinct types of MN patches were fabricated. These MN patches were systematically evaluated for their performance in skin insertion, drug loading, drug deposition, and overall delivery efficiency. The results, presented in Fig. 3-A–D, demonstrate the capability of all MN patches to breach the skin barrier and reach deeper layers. However, as depicted in Fig. 3-E, the results of the skin deposition study showed that the 14 × 14 MN patches and 19 × 19 MN patches had inadequate retention in the skin. Upon removal after 24 h of application, the tips of these MN patches were found to float on the skin surface, and no drug depots were observed. In contrast, the 600 MN patches and 16 × 16 MN patches demonstrated successful drug deposition in the skin.

Table 2
Particle sizes, PDI and zeta potential of DCF-NPs (means ± SDs, n = 3).

Parameters	Before freeze-drying	After freeze-drying
Particle size (nm)	201.35 ± 1.28	202.63 ± 2.02
PDI	0.123 ± 0.013	0.166 ± 0.017
Zeta potential (mV)	9.33 ± 0.95	12.72 ± 0.32

These MN patches, fabricated using the same DCF-NP casting formulation, but with variations in needle length, width, geometry, and number, displayed differences in drug loading. As demonstrated in Fig. 3-F, MN patches with longer needles, such as the 600 MN patches (2.33 ± 0.18 mg, means + SDs, n = 6) and 16 × 16 MN patches (2.26 ± 0.25 mg, means + SDs, n = 6), had higher drug contents, while MN patches with shorter needles exhibited lower drug loading, with 1.28 ± 0.05 mg for 14 × 14 MN patches (means + SDs, n = 6), and 1.24 ± 0.09 mg for 19 × 19 MN patches (means + SDs, n = 6). Additionally, the MN patches with longer needles demonstrated better insertion performance, allowing effective embedding in the skin to form a drug reservoir for potential prolonged drug delivery.

Further analysis revealed that the 16 × 16 MN patches (0.41 ± 0.12 mg, means + SDs, n = 4) and 600 MN patches (0.40 ± 0.08 mg, means + SDs, n = 4) exhibited comparable drug deposition in the skin, which was significantly higher than that observed with the 14 × 14 MN patches (0.22 ± 0.07 mg, means + SDs, n = 4) and 19 × 19 MN patches (0.15 ± 0.06 mg, means + SDs, n = 4) (Fig. 3-F). Delivery efficiency analysis showed no significant differences among the MN patches (17 % for 600 MN patches, 18 % for 16 × 16 MN patches, 17 % for 14 × 14 MN patches), except for the 19 × 19 MN patches (12 %), which had relatively lower efficiency (Fig. 3-F).

DCF is usually administered in large doses (100–150 mg daily) due to its rapid systemic absorption, short biological half-life, and fast elimination rate [43]. Only 60 % of DCF can reach the systemic circulation when administered orally because of first-pass metabolism. Local delivery *via* skin can avoid the first-pass metabolism of the gastrointestinal tract and provide a high local drug concentration, potentially reducing the dose requirement. MN patches with higher drug loading are preferable for practical applications. Based on the evaluation results, 600

Table 1
Particle size and PDI value after freeze-drying (means ± SDs, n = 3).

Protectants	Polymer content (%w/w)	DCF content (%w/w)	Polymer:drug	H_2O content (% w/w)	Particle size (nm)	PDI
PVP 10 K	0.96	2.75	1:3	96.29	Micron	NA
PVA 9–10 K	0.96	2.75	1:3	96.29	348.47 ± 3.31	0.190 ± 0.030
PVP 10 K & PVA 9–10 K	1.91	2.72	2:3	95.37	405.72 ± 20.22	0.267 ± 0.029
PVP 10 K & PVP 58 K	1.91	2.72	2:3	95.37	353.83 ± 7.18	0.250 ± 0.007
PVA 9–10 K & PVP 58 K	1.91	2.72	2:3	95.37	364.15 ± 3.92	0.234 ± 0.013
PVA 9–10 K & PVP 58 K	2.71	2.71	1:1	94.59	372.31 ± 4.56	0.201 ± 0.016

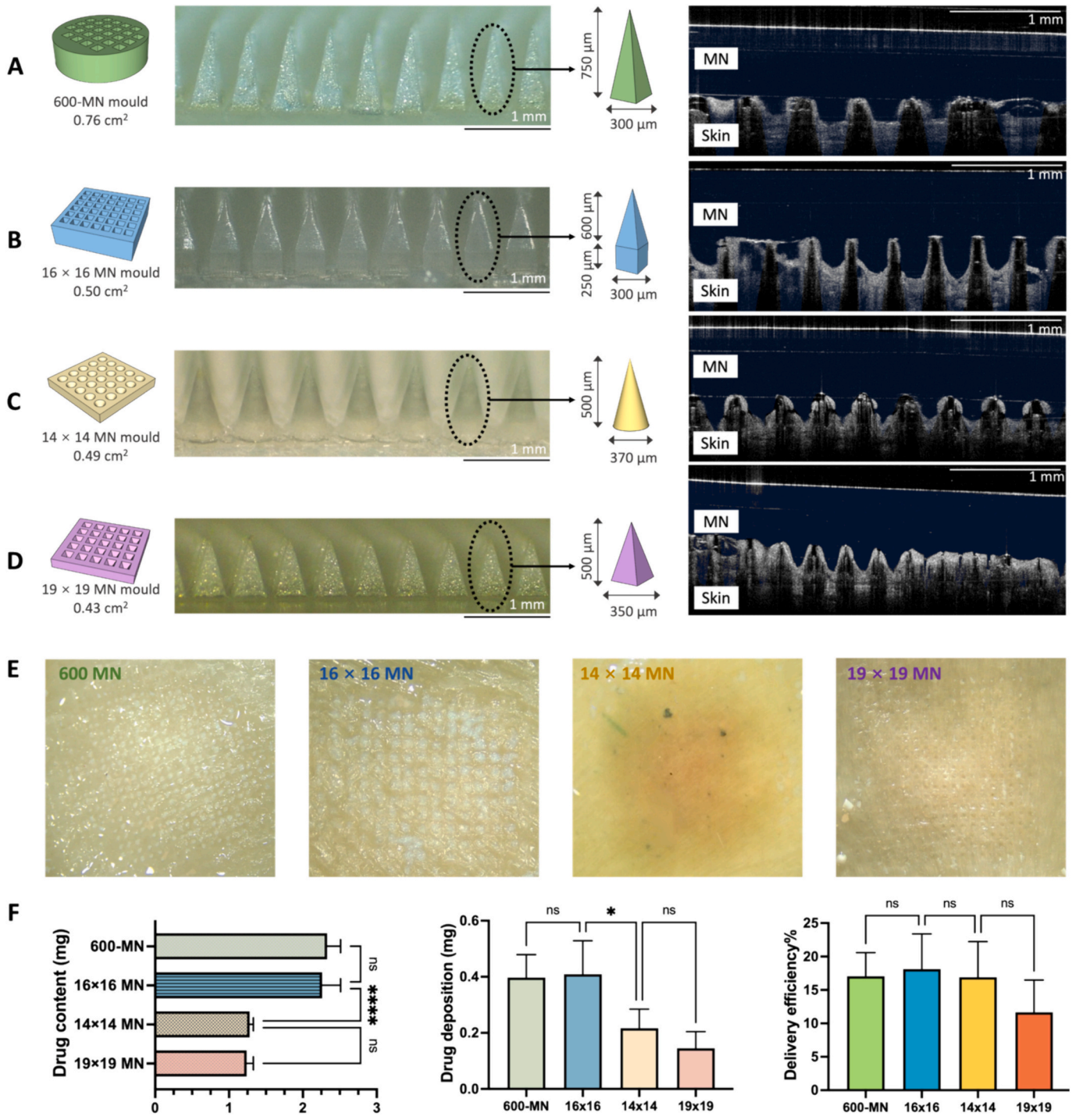

Fig. 3. Dimensions, microscopic images and skin insertion of MN patches cast from (A) 600-MN mould, (B) 16 × 16 MN mould, (C) 14 × 14 MN mould, and (D) 19 × 19 MN mould. (E) Drug depots in the skin after 24 h. (F) Drug contents, drug depositions and delivery efficiencies of different MN patches (means + SDs, $n = 6$).

MN moulds were employed for the further production of DCF MN patches.

This study provides insights into the performance of different MN patches in terms of drug loading, drug deposition, and delivery efficiency. The findings highlight the suitability of the 600 MN patches and 16 × 16 MN patches for the development of DCF MN patches, facilitating improved practical application.

3.4. Characterisation of drug-loaded MNs

Drug-loaded MN patches, fabricated using 600-MN moulds, were prepared. The resulting MN patches, containing DCF-NP (Fig. 4-A) and DCF-P (Fig. 4-B), were carefully demoulded. Subsequently, these MN patches were examined using both light microscopy and SEM for detailed morphological observation.

3.4.1. MN insertion study

The *in vitro* membrane insertion and mechanical strength of the tips of DCF-NP-loaded and DCF-P-loaded MN patches were characterised, and the results are presented in Fig. 4-C. In the insertion studies, all the needle tips of both DCF-NP MNs and DCF-P MNs penetrated the first layer of Parafilm M® with an insertion depth of 125 µm. > 80 % of the

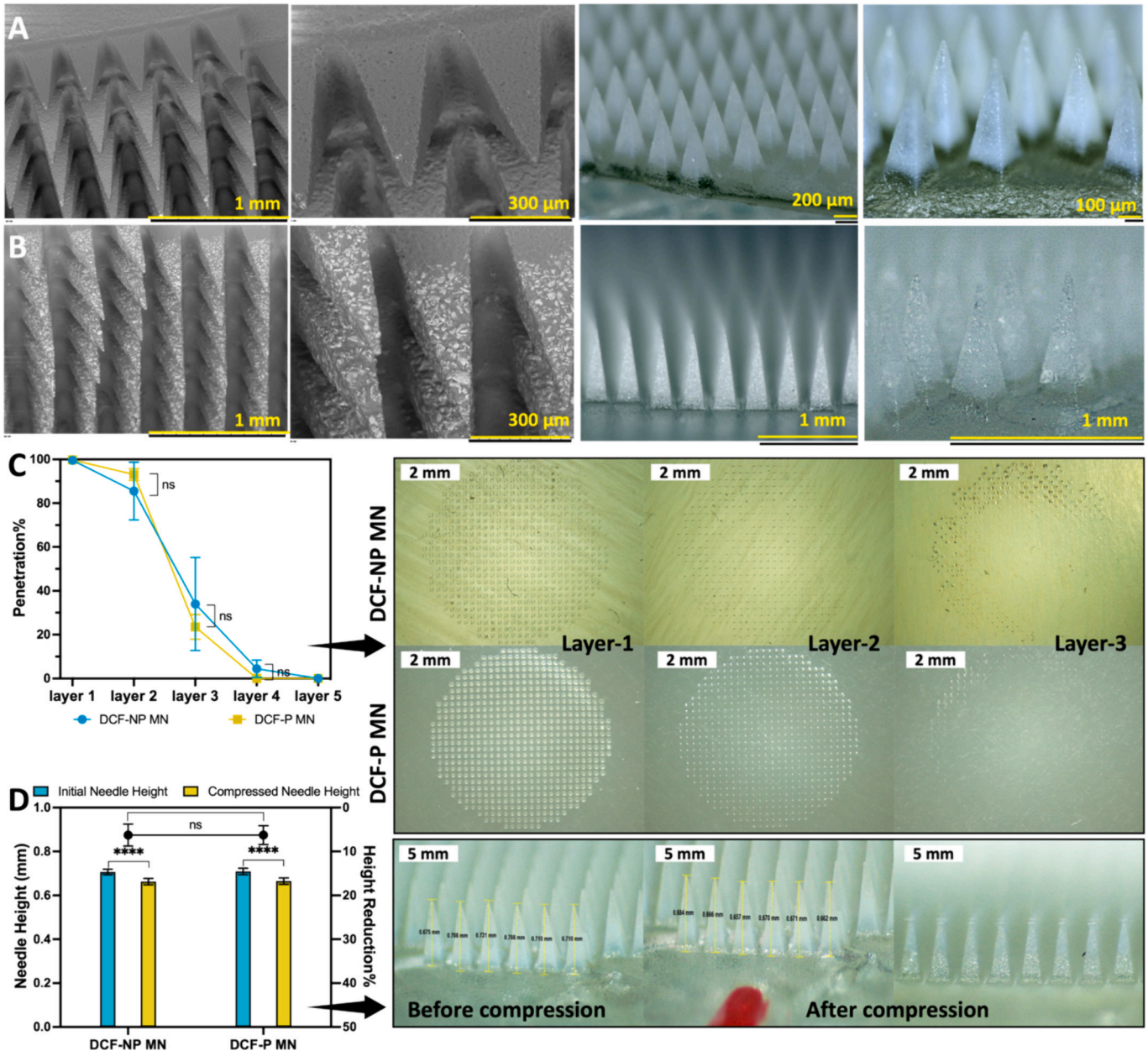

Fig. 4. Morphology of the formed 600 MN patches cast from (A) DCF-NPs and (B) DCF-P. (C) Parafilm M® insertion of DCF-NP-loaded MN patches and DCF-P-loaded MN patches (means ± SDs, $n = 3$). (D) Needle compression and height reduction of DCF-NP MNs and DCF-P MNs (means ± SDs, $n = 8$).

needle tips penetrated the second layer of Parafilm M® with an insertion depth of 250 µm, and approximately 30 % of the needle tips penetrated three layers of Parafilm M®, indicating an insertion depth of 375 µm. Larrañeta *et al.* [44] suggested that the penetration depth of MN patches was lower in Parafilm M® than in neonatal porcine skin, which is considered a simulated model of human skin in terms of hair sparseness and physical properties. Therefore, this insertion depth is sufficient to breach the skin barrier, namely, the *stratum corneum*, which is typically 10 to 20 µm thick [45], allowing for potential intradermal and transdermal drug delivery.

3.4.2. MN compression study

The needle height was measured both before and after compression to evaluate the height reduction as an indication of the mechanical strength of MN tips (Fig. 4-D). The needle tips of both DCF-NP MNs and DCF-P MNs maintained their initial shape and were not crushed or bent under the insertion force. The height reductions for both MN patches were 6.26 % and 6.24 %, respectively, indicating that the needle tips had adequate mechanical strength to penetrate the skin and deliver the drug. This is an important consideration for the commercialisation of MNs, as it ensures their practicality for clinical application, storage and transportation.

3.5. Ex vivo skin permeation study

To elucidate the differences in skin delivery properties of various DCF formulations, an *ex vivo* skin permeation study was conducted. DS, commonly employed to enhance the solubility and bioavailability of DCF, was also incorporated into the MNs for comparative analysis. This comprehensive analysis involved DCF-NP MNs, DCF-P MNs, DS MNs, and a commercial transdermal formulation Voltarol® gel, including both the acid and soluble salt forms, providing valuable insights on the efficiency of skin delivery of DCF.

Each type of MN patch utilized a casting gel with approximately 27 %

w/w of DS/DCF, although the drug content varied across the MN patches. Specifically, DS MNs exhibited a drug loading of 1.5 mg per patch, DCF-NP MNs showed 3.2 mg per patch, and DCF-P MNs had 6.7 mg per patch, as demonstrated in Fig. 5-A. All formulations were applied to 1.8 cm^2 of skin (Franz-cell donor area), and the amount of Voltarol® gel applied to the skin was quantified to be 0.8 mg (heavy gel application). The variation in drug content between MN groups can be attributed to the tendency of large DCF crystals to settle in the cavities of the MN moulds from the overloaded casting gel, leading to needle tips with a high drug content. In contrast, DS and DCF-NPs were more evenly distributed in the polymer gel, leading to MNs with consistent drug content. The nanoscale size of DCF-NPs allowed for a higher drug content in the microscale needle tips compared to DS MNs.

Fig. 5-A also presents the diagram illustrating drug release from MN patches in the skin. The MN patches were manually inserted into full-thickness neonatal porcine skin. Upon insertion, the drug-free polymer layer dissolved, and the drug-loaded tips were deposited in the skin. Following dissolution, the drugs were distributed within and then permeated across the epidermis and dermis layer to the receptor underneath the full-thickness skin, thereby mimicking the drug delivery process across human skin.

In a 24-h period, DS MNs transdermally delivered 71 % of the drug to the receptor, corresponding to a total amount of 1042.99 μg, while 7 % of the drug remained intradermally deposited in the skin, amounting to 104.70 μg (Fig. 5-C). The release of drugs from DS MNs was rapid, as illustrated in Fig. 5-B, with faster permeation across the skin compared to other DCF-loaded MNs. > 50 % of the drug was released within 8 h, and the release rate slowed down afterward.

In contrast, the drug release from DCF-P MNs exhibited a relatively consistent profile (Fig. 5-B). As shown in Fig. 5-C, within 24 h, DCF-P MNs delivered 917.17 μg of the total drug content, with 250.23 μg deposited intradermally and 666.94 μg permeated across the skin. The overall delivery efficiency was 14 % relative to the drug content in the MNs.

DCF-NP MNs demonstrated a controlled release profile (Fig. 5-B), following a similar trend as DCF-P MNs in the first 6 h, with a sustained release until 24 h. In total, 41 % of the drugs were delivered into or across the skin. Of this amount, 36 % (representing 1163.81 μg) was recovered from the receptor under the skin 24 h after application, while 5 % (at an amount of 144.88 μg) was extracted from the skin (Fig. 5-C).

The release profile of Voltarol® gel, as illustrated in Fig. 5-B, exhibited consistency. It was observed that 179.04 μg of the drug permeated across the skin and was detected in the receptor of Franz-cell. Additionally, 58 μg of the drug was found to be deposited in the skin (Fig. 5-C).

The findings of this study suggest that the use of DS MNs offers rapid onset of action, but may lead to a relatively high peak plasma concentration and a shorter effective duration after a single administration, similar to the systemic side effects associated with oral administration and the need for frequent dosing. On the other hand, DCF-P MNs have the capability to accommodate a higher drug load per patch, which is desirable for high-dose drug delivery. However, their delivery efficiencies and drug delivery amounts were significantly lower than those of the other two MN patches. One possible explanation for this

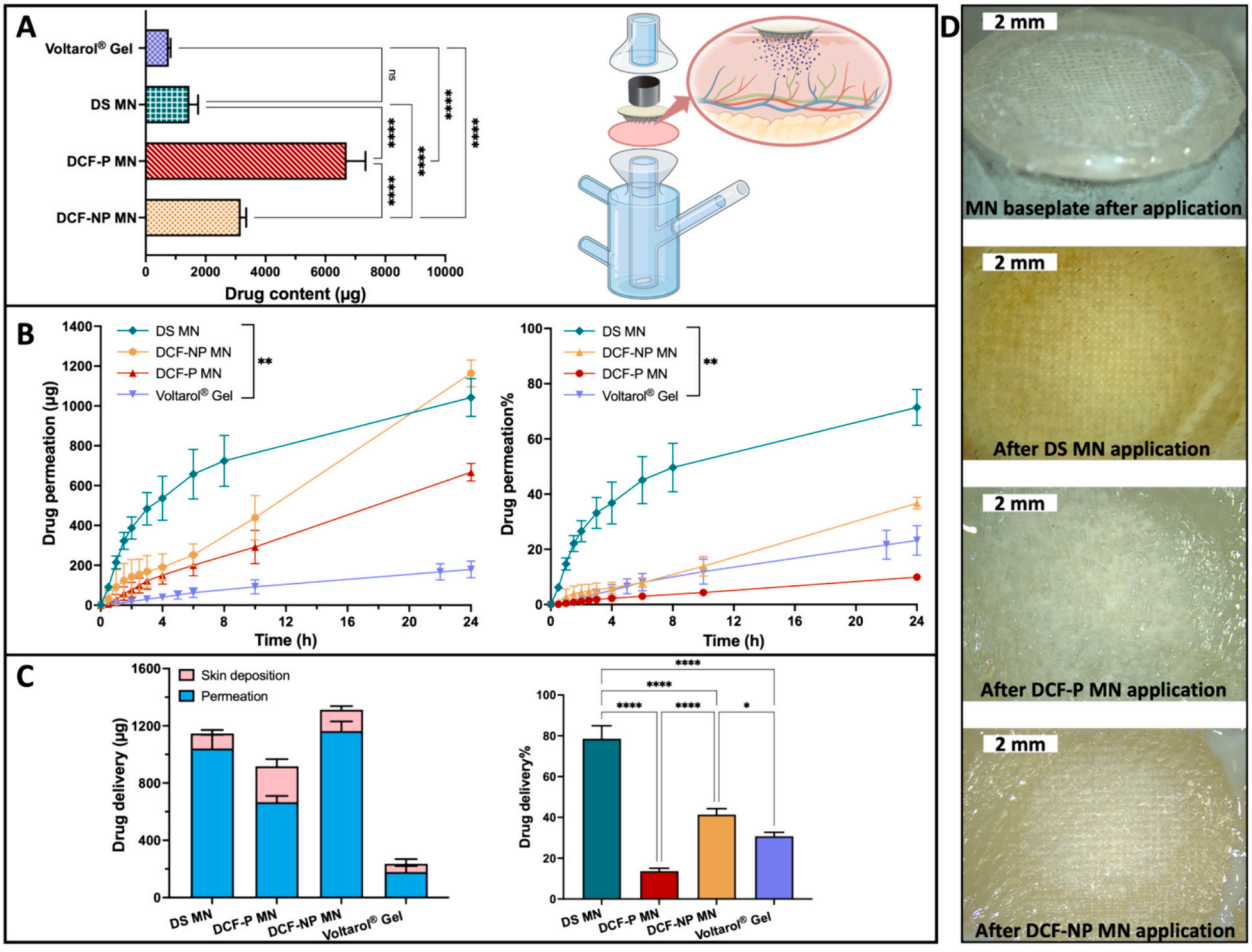

Fig. 5. (A) Drug contents of MNs and amount of drug in Voltarol® gel applied to the skin (means + SDs, $n = 5$). (B) The amount and percentage of DCF delivered across the skin from different formulations (means ± SDs, $n = 3$). (C) Drug distribution and drug delivery efficiencies of different DCF formulations in *ex vivo* Franz-cell studies (means + SDs, $n = 3$). (D) Microscopic photos of skins after 24 h of application of different types of MN patches.

observation could be the challenges associated with the deposition and dissolution of large DCF drug crystals within the skin. Specifically, after 24 h of application, drug crystals were observed on the skin surface, as depicted in Fig. 5-D, which may originate from the needle tips above the skin (uninserted part) or the drug depot within the skin. Due to the large size and hydrophobic nature of DCF, these drug crystals deposited in the skin were not easily dispersed or dissolved, and they may tend to be expelled from the skin through the microchannels created by the MNs. In contrast, DCF-NP MNs exhibited a moderate drug load per MN patch, making them more practical for high-dose drug delivery. Moreover, localised application allows for higher concentrations at the target site and bypasses first-pass metabolism by the gastrointestinal tract, potentially reducing the required dose compared to oral administration. Furthermore, DCF-NP MNs demonstrated a controlled release profile at a relatively consistent rate. When combined with the drug depot in the skin after 24 h, this profile indicates the potential for prolonged delivery of DCF. The topical formulation Voltarol® gel demonstrated a lower drug delivery capacity, both in terms of the amount of drug delivered and the efficiency of delivery, when compared to the DS MNs or DCF-NP MNs.

Based on the evaluation of drug loading, drug delivery amount and efficiency, as well as the *ex vivo* release profile of different DCF form-loaded MN patches, DCF-NP MNs were used for further investigation in an animal study to explore their *in vivo* pharmacokinetics to compare with oral formulation of DCF.

3.6. In vivo pharmacokinetics and drug distribution

MN patches were applied to the dorsal skin of rats, which were then securely wrapped to prevent removal, as illustrated in Fig. 6-A. After 24 h of application, the MN patches were removed. As shown in Fig. 6-B, the MN tips were observed to be completely dissolved, and a blank baseplate was left on the adhesive tape. The skin of the rats showed no visible drug or polymer residue, and the white drug deposition in the rat dorsal skin was clearly observed. No noticeable skin irritation was observed, such as redness, rash, dryness, peeling, itching, or edema.

Plasma concentrations of DCF were quantified to evaluate the pharmacokinetics (PK) of DCF-NP MNs and the results are present in Fig. 6-C. The PK analysis was conducted using a noncompartmental model, and the PK parameters are listed in Table 3. The PK parameters for each experimental rat are reported in Supplementary S.5. Table 4. The drug distribution in the skin, muscle and paw was assessed at 24 and 72 h after MN application, as shown in Fig. 6-C. The synthesis of prostaglandins (particularly PGE_2) is a surrogate for COX-2 activity; therefore, inhibition of PGE_2 by DCF can be considered an indicator of COX-2 inhibition [44,46]. Research on therapeutically active concentrations of DCF is limited, and the results are highly variable. Hagen *et al.* (2017) calculated the IC_{50} (50 % of the maximum inhibition of prostaglandin synthesis) of DCF reported in previous studies and found that the *in vivo* IC_{50} level for DCF was 45 ng/mL and IC_{80} was >100 ng/mL [47–49]. The reported *in vivo* IC_{50} levels are significantly higher than the *in vitro* assessed IC_{50} levels (range 0.47–21 ng/mL) [50–56]. In the current

Table 3
Systemic PK analysis of the *in vivo* study (means ± SDs, n = 4).

PK parameter	Unit	Oral group	MN group
$T_{1/2}$	h	1.9 ± 0.8	8.7 ± 4.0
T_{max}	h	1	1
C_{max}	ng/mL	3690.6 ± 1058.9	2531.1 ± 770.9
AUC $_{0\text{-}t}$	ng/mL*h	7935.4 ± 1129.8	30,543.9 ± 4719.7
MRT $_{0\text{-}\infty}$	h	3.2 ± 1.3	18.2 ± 4.1

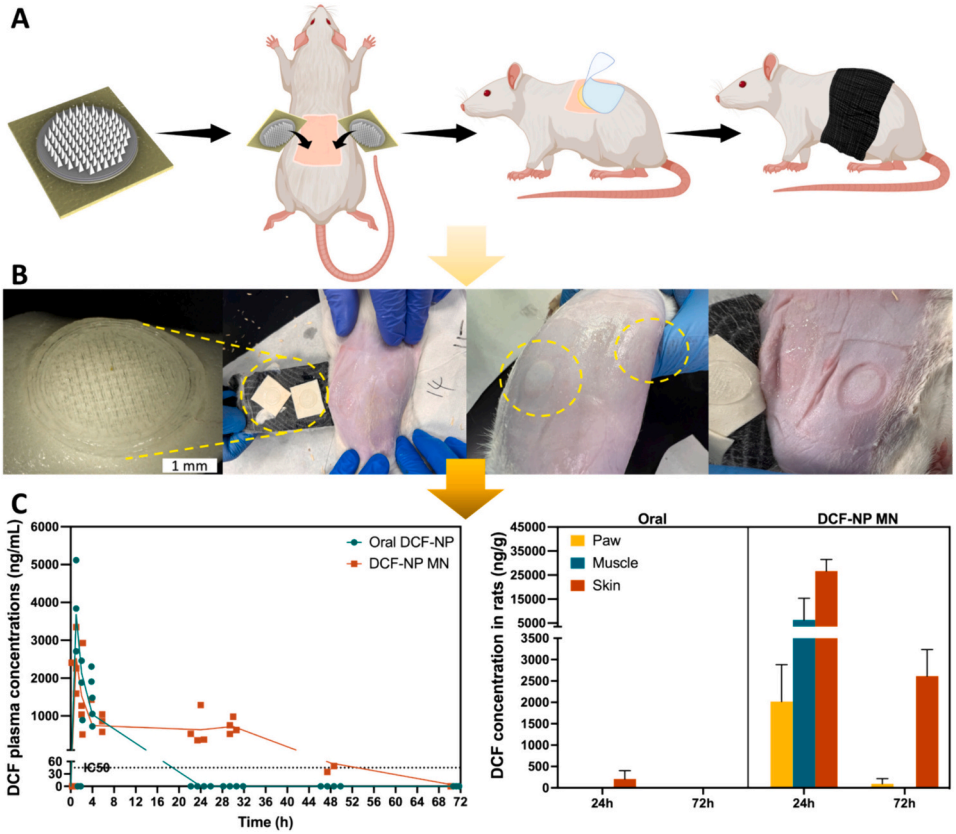

Fig. 6. (A) Diagram of MN application in rats. (B) Digital and microscopic photos at 24 h after the application of DCF-NP MNs showing MN baseplates with completely dissolved tips, MN application site after removal of the wrap and MN baseplate, and drug depots in the skin. (C) Concentration-time curve of DCF-NP MNs and oral DCF-NPs (means + SDs, $n = 4$) and drug distribution in rats after MN application and oral administration (means + SDs, $n = 3$).

study, 45 ng/mL was selected as the IC_{50} level for DCF to indicate the duration of therapeutic effects.

In the oral group, DCF exhibited a relatively short half-life ($T_{1/2}$), consistent with previous studies reporting a $T_{1/2}$ of 1 to 2 h for oral DCF [57–59]. In contrast, DCF-NP MNs showed a longer $T_{1/2}$ of 8.7 ± 4.0 h and a lower plasma C_{max} observed 1 h after MN application. The mean residence time (MRT) of DCF in rats administered DCF-NP MNs was 18.2 h, compared to 3.2 h with oral administration.

Based on the plasma concentration-time curve of DCF (Fig. 6-C), the oral group maintained plasma drug levels above the IC_{50} for < 16 h after a single administration. It should be noted that the accuracy of this value may be affected due to the limited sampling points between 4 and 24 h, in accordance with the 3Rs principle. The recommended dosing frequency of oral DCF, 2 to 3 times daily, may suggest a duration of therapeutic effects of approximately 8 to 12 h, which aligns with our experimental findings [60,62]. In comparison, the DCF-NP MN group exhibited a similar rapid absorption and onset of action time (T_{max} of 1 h) as the oral group. However, in contrast to the short duration of therapeutic activity observed with oral administration, the DCF-NP MN group demonstrated an extended drug plasma level (> IC_{50}) for up to 48 h after a single administration. Analysis of the plasma concentration-time curve revealed a constant concentration of DCF between 4 and 30 h following MN administration, indicating a dynamic equilibrium between absorption and elimination processes during this 4–30 h timeframe. Subsequently, DCF was gradually eliminated from the body.

Additionally, the distribution of DCF in various tissues was assessed at 24 and 72 h post-administration. In the oral group, DCF was detected in the skin after 24 h, with a mean concentration of 206.96 ng/g ± 194.157 ng/g (mean ± SD, $n = 3$), suggesting possible distribution through the skin microcirculation [47]. However, no DCF was found in the muscles or paws at 24 or 72 h. In contrast, the MN group exhibited substantial local concentrations of DCF at the application site 24 h after a single administration. A drug reservoir containing a total of 26,726.10 ng/g DCF was observed in the skin at the application site, while the muscles underneath the applied skin site contained 6330.43 ng/g DCF. Remarkably, even after 72 h, DCF was still detected in the skin with a mean concentration of 2614.84 ng/g. Interestingly, DCF distribution was also observed in the paws of rats in the DCF-NP MN group. After 24 h of MN application, 2020.03 ng/g DCF was recovered from the paws and, after 72 h, a mean concentration of 96.65 ng/g was still detected. This distinct distribution pattern was not observed in the oral group.

The findings from this study provide evidence for the potential of DCF-NP MNs as a promising formulation for achieving prolonged therapeutic effects with an improved PK profile. DCF-NP MNs exhibited a lower peak plasma concentration (C_{max}) and maintained somewhat more stable plasma drug levels, indicating a controlled and sustained release of the drug. Additionally, DCF-NP MNs formed drug reservoirs in the skin, resulting in sustained local concentrations of the drug for up to 72 h. Notably, the successful delivery of DCF to the paws of rats highlighted the potential of DCF-NP MNs in achieving prolonged drug delivery at the desired site for up to 72 h. In comparison to systemic delivery through oral administration, DCF-NP MNs demonstrated advantageous characteristics in terms of targeted and sustained drug release, suggesting their potential as a preferred approach for optimised therapeutic outcomes.

The relative systemic bioavailability (F) of DCF-NP MNs, determined using Eq. (1), was found to be 57 % compared to the oral formulation. This indicates that, on average, 57 % of the administered DCF from the applied DCF-NP MNs was systemically absorbed, which is higher than the relative bioavailability of 6 % reported for Voltaren® gel, a widely marketed commercial product [61].

The oral bioavailability of DCF has been previously reported to be approximately 60 % [57,61], which served as the basis for calculating the delivery efficiency of DCF-NP MNs using Eq. (2). The calculated delivery efficiency of DCF-NP MNs was found to be 34 %, representing the fraction of the administered dose that reaches the systemic circulation. In comparison, while the systemic bioavailability of DCF *via* oral routes is slightly higher, the advantages of localised, prolonged delivery and reduced systemic exposure offered by DCF-NP MNs highlight their potential in clinical settings where reducing systemic side effects is desired. The MN patches' ability to directly deliver the drug to specific sites further exemplifies this point, illustrating their capacity for precise targeting without the need for higher, more frequent dosing associated with oral drugs.

Overall, the application of DCF-NP MNs could revolutionize the approach to treating conditions that benefit from localised and controlled drug delivery systems, such as chronic pain management in osteoarthritis, by optimizing therapeutic outcomes and minimizing systemic impacts. This aligns with ongoing trends in pharmaceutical technology that seek to improve patient compliance and efficacy through innovative drug delivery platforms.

4. Conclusions

The current study showed that a single application of DCF-NP MNs could provide up to 48 h of systemic delivery and up to 72 h of localised and target drug concentrations. These results indicate that DCF-NP MNs are a promising strategy for DCF administration in OA treatment, with higher bioavailability than oral formulations, long-term delivery and extended therapeutic activity, as well as potentially better safety. The present study has shown promising outcomes regarding the skin delivery of DCF. However, further preclinical investigations are necessary to fully understand the pharmacodynamics of DCF-NP MNs and evaluate their therapeutic efficacy comprehensively. Moreover, assessing the long-term efficacy and safety of the developed delivery system in larger animal models is essential to establish its potential as an improved treatment option for OA. Additionally, exploring the use of DCF-NP MNs in combination therapy with other anti-inflammatory agents could be valuable in enhancing therapeutic outcomes.

Abbreviations

AUC	Area under the curve
ANOVA	Analysis of variance
COX-1	Cyclooxygenase-1 enzyme
COX-2	Cyclooxygenase-2 enzyme
C_{max}	Peak plasma concentration
DCF	Diclofenac
DCF-NP	Diclofenac nanoparticle
DS	Diclofenac sodium
DCF-P	Diclofenac coarse powder
F	The relative systemic bioavailability
GI	Gastrointestinal
IC_{50}	50 % of the maximum inhibition of prostaglandin synthesis
MN	Microneedle
MRT	Mean residence time
NICE	National Institute of Clinical Excellence
NSAID	Nonsteroidal anti-inflammatory drug
OA	Osteoarthritis
OCT	Optical coherence tomography
PVA	Poly(vinyl alcohol)
PVP	Plasdone™, Povidone
PBS	Phosphate buffered saline
PDI	Polydispersity index
PK	Pharmacokinetics
SEM	Scanning electron microscopy
$T_{1/2}$	Half-life
T_{50}	Time to release 50 % of drug
T_{80}	Time to release 80 % of drug

Ethics approval and consent to participate

The Committee of Biological Service Unit at Queen's University Belfast granted approval for the animal experiments conducted in this study under Project Licence PPL 2903 and Personal Licences PIL 1892, PIL 2056 and PIL 2154. All animal experiments were conducted in accordance with the 3Rs principle (replacement, reduction and refinement).

Consent for publication

Not applicable.

Funding

We acknowledge the funding support from Queen's University Belfast and the China Scholarship Council.

CRediT authorship contribution statement

Mingshan Li: Writing – review & editing, Writing – original draft, Visualization, Validation, Methodology, Investigation, Formal analysis, Data curation. **Lalitkumar K. Vora:** Writing – review & editing, Visualization, Supervision, Resources, Investigation, Conceptualization. **Ke Peng:** Methodology, Investigation. **Akmal H.B. Sabri:** Writing – review & editing, Methodology. **Nuoya Qin:** Methodology. **Marco Abbate:** Writing – review & editing, Methodology, Formal analysis. **Alejandro J. Paredes:** Writing – review & editing, Methodology, Formal analysis. **Helen O. McCarthy:** Resources, Methodology, Investigation, Formal analysis. **Ryan F. Donnelly:** Writing – review & editing, Visualization, Supervision, Resources, Project administration, Funding acquisition, Conceptualization.

Declaration of competing interest

Ryan Donnelly is an inventor of patents that have been licenced to companies developing microneedle-based products and is a paid advisor to companies developing microneedle-based products. The resulting potential conflict of interest has been disclosed and is managed by Queen's University Belfast. The companies had no role in the design of the present studies, in the collection, analyses or interpretation of the data, in the writing of the manuscript or in the decision to publish the work.

Other all authors declare that they have no known competing financial interests or personal relationships that could have appeared to influence the work reported in this paper.

Availability of data and materials

The datasets used and analysed in this study are available upon reasonable request.

Acknowledgement

We acknowledge the Committee of Biological Service Unit at Queen's University Belfast and Professor Helen McCarthy for their support of animal study.

Appendix A. Supplementary data

Supplementary data to this article can be found online at https://doi.org/10.1016/j.bioadv.2024.213889.

References

[1] D. Scott, A. Kowalczyk, Osteoarthritis of the knee, BMJ Clinical Evidence 2007 (2007) 51–59, https://doi.org/10.1056/NEJMcp1903768.
[2] L. Tong, H. Yu, X. Huang, J. Shen, G. Xiao, L. Chen, H. Wang, L. Xing, D. Chen, Current understanding of osteoarthritis pathogenesis and relevant new approaches, Bone Research 10 (2022) 60.
[3] E.R. Vina, C.K. Kwoh, Epidemiology of osteoarthritis: literature update, Curr. Opin. Rheumatol. 30 (2018) 160–167, https://doi.org/10.1097/BOR.0000000000000479.
[4] N. Gerwin, C. Scotti, C. Halleux, M. Fornaro, J. Elliott, Y. Zhang, K. Johnson, J. Shi, S. Walter, Y. Li, C. Jacobi, N. Laplanche, M. Belaud, J. Paul, G. Glowacki, T. Peters, K.A. Wharton, I. Vostiar, F. Polus, I. Kramer, S. Guth, A. Seroutou, S. Choudhury, D. Laurent, J. Gimbel, J. Goldhahn, M. Schieker, S. Brachat, R. Roubenoff, M. Kneissel, Angiopoietin-like 3-derivative LNA043 for cartilage regeneration in osteoarthritis: a randomized phase 1 trial, Nat. Med. 28 (2022) 2633–2645, https://doi.org/10.1038/s41591-022-02059-9.
[5] N. guideline NG226, Osteoarthritis in Over 16s: Diagnosis and Management, 2022.
[6] R.R. Bannuru, M.C. Osani, E.E. Vaysbrot, N.K. Arden, K. Bennell, S.M.A. Bierma-Zeinstra, V.B. Kraus, L.S. Lohmander, J.H. Abbott, M. Bhandari, OARSI guidelines for the non-surgical management of knee, hip, and polyarticular osteoarthritis, Osteoarthr. Cartil. 27 (2019) 1578–1589.
[7] K. Chen, X. Mao, M. Yu, W. Zhou, S. Shang, Microneedling in the relief of pain in arthritis: a brief review, Interdisciplinary Nursing Research (2023) 121–129, https://doi.org/10.1097/NR9.0000000000000027.
[8] K. Yu, X. Yu, S. Cao, Y. Wang, Y. Zhai, F. Yang, X. Yang, Y. Lu, C. Wu, Y. Xu, Layered dissolving microneedles as a need-based delivery system to simultaneously alleviate skin and joint lesions in psoriatic arthritis, Acta Pharm. Sin. B (2021) 505–519, https://doi.org/10.1016/j.apsb.2020.08.008.
[10] G. Honvo, V. Leclercq, A. Geerinck, T. Thomas, N. Veronese, A. Charles, V. Rabenda, C. Beaudart, C. Cooper, J.-Y. Reginster, Safety of topical non-steroidal anti-inflammatory drugs in osteoarthritis: outcomes of a systematic review and meta-analysis, Drugs Aging 36 (2019) 45–64.
[11] A. Fini, G. Fazio, M. Gonzalez-Rodriguez, C. Cavallari, N. Passerini, L. Rodriguez, Formation of ion-pairs in aqueous solutions of diclofenac salts, Int. J. Pharm. 187 (1999) 163–173, https://doi.org/10.1016/S0378-5173(99)00180-5.
[12] L.K. Vora, A.H. Sabri, Y. Naser, A. Himawan, A.R.J. Hutton, Q.K. Anjani, F. Volpe-Zanutto, D. Mishra, M. Li, A.M. Rodgers, A.J. Paredes, E. Larrañeta, R.R.S. Thakur, R.F. Donnelly, Long-acting microneedle formulations, Adv. Drug Deliv. Rev. 201 (2023) 115055, https://doi.org/10.1016/j.addr.2023.115055.
[13] S. Abdelghany, I.A. Tekko, L. Vora, E. Larrañeta, A.D. Permana, R.F. Donnelly, Nanosuspension-based dissolving microneedle arrays for intradermal delivery of curcumin, Pharmaceutics 11 (2019) 308, https://doi.org/10.3390/pharmaceutics11070308.
[14] L.K. Vora, R.F. Donnelly, E. Larrañeta, P. González-Vázquez, R.R.S. Thakur, P. R. Vavia, Novel bilayer dissolving microneedle arrays with concentrated PLGA nano-microparticles for targeted intradermal delivery: proof of concept, J. Control. Release 265 (2017) 93–101.
[15] M.I. Nasiri, L.K. Vora, Juhaina, A. Ershaid, Ke Peng, I.A. Tekko, R.F. Donnelly, Nanoemulsion-based dissolving microneedle arrays for enhanced intradermal and transdermal delivery, Drug Deliv Transl Res 1 (n.d.) 3. doi:https://doi.org/10.1007/s13346-021-01107-0.
[16] I.A. Tekko, A.D. Permana, L. Vora, T. Hatahet, H.O. McCarthy, R.F. Donnelly, Localised and sustained intradermal delivery of methotrexate using nanocrystal-loaded microneedle arrays: potential for enhanced treatment of psoriasis, Eur. J. Pharm. Sci. 152 (2020) 105469.
[17] E. Larrañeta, L. Vora, Delivery of nanomedicines using microneedles, Microneedles for Drug and Vaccine Delivery and Patient Monitoring (2018) 177–205.
[18] E. Altuntaş, I.A. Tekko, L.K. Vora, N. Kumar, R. Brodsky, O. Chevallier, E. McAlister, Q.K. Anjani, H.O. McCarthy, R.F. Donnelly, Nestorone nanosuspension-loaded dissolving microneedles array patch: a promising novel approach for "on-demand" hormonal female-controlled peritcoital contraception, Int. J. Pharm. 614 (2022) 121422, https://doi.org/10.1016/j.ijpharm.2021.121422.
[19] L.K. Vora, K. Moffatt, R.F. Donnelly, Long-lasting drug delivery systems based on microneedles, in: Long-acting Drug Delivery Systems, Elsevier, 2022, pp. 249–287.
[20] A.J. Paredes, F. Volpe-Zanutto, L.K. Vora, I.A. Tekko, A.D. Permana, C.J. Picco, H. O. McCarthy, R.F. Donnelly, Systemic delivery of tenofovir alafenamide using dissolving and implantable microneedle patches, Mater Today Bio 13 (2022) 100217.
[21] H.S. Faizi, L.K. Vora, M.I. Nasiri, Y. Wu, D. Mishra, Q.K. Anjani, A.J. Paredes, R.R. S. Thakur, M.U. Minhas, R.F. Donnelly, Deferasirox nanosuspension loaded dissolving microneedles for intradermal delivery, Pharmaceutics 14 (2022), https://doi.org/10.3390/pharmaceutics14122817.
[22] A.J. Guillot, M. Martínez-Navarrete, V. Zinchuk-Mironova, A. Melero, Microneedle-assisted transdermal delivery of nanoparticles: recent insights and prospects, Wiley Interdiscip. Rev. Nanomed. Nanobiotechnol. (2023) 1–30, https://doi.org/10.1002/wnan.1884.
[23] R. Pireddu, M. Schlich, S. Marceddu, D. Valenti, E. Pini, A.M. Fadda, F. Lai, C. Sinico, Nanosuspensions and microneedles roller as a combined approach to enhance diclofenac topical bioavailability, Pharmaceutics 12 (2020) 1–14, https://doi.org/10.3390/pharmaceutics12121140.
[24] Y. Wu, L.K. Vora, D. Mishra, M.F. Adrianto, S. Gade, A.J. Paredes, R.F. Donnelly, T. R.R. Singh, Nanosuspension-loaded dissolving bilayer microneedles for hydrophobic drug delivery to the posterior segment of the eye, Biomaterials Advances 137 (2022) 212767, https://doi.org/10.1016/j.bioadv.2022.212767.

[25] A.D. Permana, A.J. Paredes, F. Volpe-Zanutto, Q.K. Anjani, E. Utomo, R. F. Donnelly, Dissolving microneedle-mediated dermal delivery of itraconazole nanocrystals for improved treatment of cutaneous candidiasis, Eur. J. Pharm. Biopharm. 154 (2020) 50–61, https://doi.org/10.1016/j.ejpb.2020.06.025.
[26] I.A. Tekko, L.K. Vora, F. Volpe-Zanutto, K. Moffatt, C. Jarrahian, H.O. McCarthy, R. F. Donnelly, Novel bilayer microarray patch-assisted long-acting Micro-depot cabotegravir intradermal delivery for HIV pre-exposure prophylaxis, Adv. Funct. Mater. 32 (2022) 2106999.
[27] L.K. Vora, I.A. Tekko, F.V. Zanutto, A. Sabri, R.K.M. Choy, J. Mistilis, P. Kwarteng, C. Jarrahian, H.O. McCarthy, R.F. Donnelly, A bilayer microarray patch (MAP) for HIV pre-exposure prophylaxis: the role of MAP designs and formulation composition in enhancing long-acting drug delivery, Pharmaceutics 16 (2024), https://doi.org/10.3390/pharmaceutics16010142.
[28] A.S. Cordeiro, I.A. Tekko, M.H. Jomaa, L. Vora, E. McAlister, F. Volpe-Zanutto, M. Nethery, P.T. Baine, N. Mitchell, D.W. McNeill, Two-photon polymerisation 3D printing of microneedle array templates with versatile designs: application in the development of polymeric drug delivery systems, Pharm. Res. 37 (2020) 1–15.
[29] A.J. Paredes, A.D. Permana, F. Volpe-Zanutto, M.N. Amir, L.K. Vora, I.A. Tekko, N. Akhavein, A.D. Weber, E. Larrañeta, R.F. Donnelly, Ring inserts as a useful strategy to prepare tip-loaded microneedles for long-acting drug delivery with application in HIV pre-exposure prophylaxis, Mater. Des. 224 (2022) 111416, https://doi.org/10.1016/j.matdes.2022.111416.
[30] M. Li, L.K. Vora, K. Peng, R.F. Donnelly, Trilayer microneedle array assisted transdermal and intradermal delivery of dexamethasone, Int. J. Pharm. 612 (2022) 121295, https://doi.org/10.1016/j.ijpharm.2021.121295.
[31] S. Rojekar, L.K. Vora, I.A. Tekko, F. Volpe-Zanutto, H.O. McCarthy, P.R. Vavia, R. F. Donnelly, Etravirine-loaded dissolving microneedle arrays for long-acting delivery, Eur. J. Pharm. Biopharm. 165 (2021) 41–51.
[32] K. Peng, L.K. Vora, I.A. Tekko, A.D. Permana, J. Domínguez-Robles, D. Ramadon, P. Chambers, H.O. McCarthy, E. Larrañeta, R.F. Donnelly, Dissolving microneedle patches loaded with amphotericin B microparticles for localised and sustained intradermal delivery: potential for enhanced treatment of cutaneous fungal infections, J. Control. Release 339 (2021) 361–380, https://doi.org/10.1016/j.jconrel.2021.10.001.
[33] R.F. Donnelly, T.R.R. Singh, D.I.J. Morrow, A.D. Woolfson, Microneedle-mediated Transdermal and Intradermal Drug Delivery, John Wiley & Sons, 2012.
[34] Y. Zhang, M. Huo, J. Zhou, S. Xie, PKSolver: an add-in program for pharmacokinetic and pharmacodynamic data analysis in Microsoft Excel, Comput. Methods Prog. Biomed. 99 (2010) 306–314, https://doi.org/10.1016/j.cmpb.2010.01.007.
[35] R.H. Müller, K. Peters, Nanosuspensions for the formulation of poorly soluble drugs. I. Preparation by a size-reduction technique, Int. J. Pharm. 160 (1998) 229–237, https://doi.org/10.1016/S0378-5173(97)00311-6.
[36] K.R. Ward, P. Matejtschuk, The principles of freeze-drying and application of analytical technologies, in: W.F. Wolkers, H. Oldenhof (Eds.), Cryopreservation and Freeze-drying Protocols, Springer US, New York, NY, 2021: pp. 99–127. doi: https://doi.org/10.1007/978-1-0716-0783-1_3.
[38] W. Abdelwahed, G. Degobert, H. Fessi, Investigation of nanocapsules stabilization by amorphous excipients during freeze-drying and storage, Eur. J. Pharm. Biopharm. 63 (2006) 87–94, https://doi.org/10.1016/j.ejpb.2006.01.015.
[39] U. Rockinger, M. Funk, G. Winter, Current approaches of preservation of cells during (freeze-) drying, J. Pharm. Sci. 110 (2021) 2873–2893, https://doi.org/10.1016/j.xphs.2021.04.018.
[40] M.R. Prausnitz, Engineering microneedle patches for vaccination and drug delivery to skin, Annu. Rev. Chem. Biomol. Eng. 8 (2017) 177–200.
[41] E. Larraneta, R.E.M. Lutton, A.D. Woolfson, R.F. Donnelly, Microneedle arrays as transdermal and intradermal drug delivery systems: materials science, manufacture and commercial development, Mater. Sci. Eng. R. Rep. 104 (2016) 1–32.
[42] A.S. Cordeiro, I.A. Tekko, M.H. Jomaa, L. Vora, E. McAlister, F. Volpe-Zanutto, M. Nethery, P.T. Baine, N. Mitchell, D.W. McNeill, R.F. Donnelly, Two-photon polymerisation 3D printing of microneedle array templates with versatile designs: application in the development of polymeric drug delivery systems, Pharm. Res. 37 (2020) 174, https://doi.org/10.1007/s11095-020-02887-9.
[43] R. Altman, B. Bosch, K. Brune, P. Patrignani, C. Young, Advances in NSAID development: evolution of diclofenac products using pharmaceutical technology, Drugs 75 (2015) 859–877, https://doi.org/10.1007/s40265-015-0392-z.
[44] E. Larrañeta, J. Moore, E.M. Vicente-Pérez, P. González-Vázquez, R. Lutton, A. D. Woolfson, R.F. Donnelly, A proposed model membrane and test method for microneedle insertion studies, Int. J. Pharm. 472 (2014) 65–73, https://doi.org/10.1016/j.ijpharm.2014.05.042.
[45] J. Torin Huzil, S. Sivaloganathan, M. Kohandel, M. Foldvari, Drug delivery through the skin: molecular simulations of barrier lipids to design more effective noninvasive dermal and transdermal delivery systems for small molecules, biologics, and cosmetics, Wiley Interdiscip. Rev. Nanomed. Nanobiotechnol. 3 (2011) 449–462.
[46] P. Patrignani, M.R. Panara, A. Greco, O. Fusco, C. Natoli, S. Iacobelli, F. Cipollone, A. Ganci, C. Creminon, J. Maclouf, Biochemical and pharmacological characterization of the cyclooxygenase activity of human blood prostaglandin endoperoxide synthases, J. Pharmacol. Exp. Ther. 271 (1994) 1705–1712.
[47] M. Hagen, M. Baker, Skin penetration and tissue permeation after topical administration of diclofenac, Curr. Med. Res. Opin. 33 (2017) 1623–1634, https://doi.org/10.1080/03007995.2017.1352497.
[48] K. Chlud, H.H. Wagener, Percutaneous therapy with non-steroidal anti-inflammatory drugs, Pharmacokinetic criteria of effectiveness, Fortschritte Der Medizin 109 (1991) 59–60.
[49] H. Liauw, S. Waiter, L. Lee, E. Ku, Effects of diclofenac on synovial eicosanoid product formation in arthritic patients, in: Journal of Clinical Pharmacology, Lippincott-Raven Publ, 227 East Washington SQ, Philadelphia, PA 19106, 1985, p. 456.
[50] J.A. Cordero, M. Camacho, R. Obach, J. Domenech, L. Vila, *In vitro* based index of topical anti-inflammatory activity to compare a series of NSAIDs, Eur. J. Pharm. Biopharm. 51 (2001) 135–142.
[51] M. Kato, S. Nishida, H. Kitasato, N. Sakata, S. Kawai, Cyclooxygenase-1 and cyclooxygenase-2 selectivity of non-steroidal anti-inflammatory drugs: investigation using human peripheral monocytes, J. Pharm. Pharmacol. 53 (2001) 1679–1685.
[52] D. Riendeau, M.D. Percival, C. Brideau, S. Charleson, D. Dube, D. Ethier, J.-P. Falgueyret, R.W. Friesen, R. Gordon, G. Greig, Etoricoxib (MK-0663): preclinical profile and comparison with other agents that selectively inhibit cyclooxygenase-2, J. Pharmacol. Exp. Ther. 296 (2001) 558–566.
[53] F. Giuliano, T.D. Warner, *Ex vivo* assay to determine the cyclooxygenase selectivity of non-steroidal anti-inflammatory drugs, Br. J. Pharmacol. 126 (1999) 1824–1830.
[54] T.D. Warner, F. Giuliano, I. Vojnovic, A. Bukasa, J.A. Mitchell, J.R. Vane, Nonsteroid drug selectivities for cyclo-oxygenase-1 rather than cyclo-oxygenase-2 are associated with human gastrointestinal toxicity: a full *in vitro* analysis, Proc. Natl. Acad. Sci. 96 (1999) 7563–7568.
[55] B. Cryer, M. Feldman, Cyclooxygenase-1 and cyclooxygenase-2 selectivity of widely used nonsteroidal anti-inflammatory drugs, Am. J. Med. 104 (1998) 413–421.
[56] M. Pairet, J. Van Ryn, H. Schierok, A. Mauz, G. Trummlitz, G. Engelhardt, Differential inhibition of cyclooxygenases-1 and-2 by meloxicam and its 4′-isomer, Inflamm. Res. 47 (1998) 270–276.
[57] J.V. Willis, M.J. Kendall, R.M. Flinn, D.P. Thornhill, P.G. Welling, The pharmacokinetics of diclofenac sodium following intravenous and oral administration, Eur. J. Clin. Pharmacol. 16 (1979) 405–410, https://doi.org/10.1007/BF00568201.
[58] N.M. Davies, K.E. Anderson, Clinical pharmacokinetics of diclofenac, Clin. Pharmacokinet. 33 (1997) 184–213, https://doi.org/10.2165/00003088-199733030-00003.
[59] B. Hinz, J. Chevts, B. Renner, H. Wuttke, T. Rau, A. Schmidt, I. Szelenyi, K. Brune, U. Werner, Bioavailability of diclofenac potassium at low doses, Br. J. Clin. Pharmacol. 59 (2005) 80–84, https://doi.org/10.1111/j.1365-2125.2005.02226.x.
[60] Joint Formulary Committee, British National Formulary London: BMJ Group and Pharmaceutical Press. http://www.medicinescomplete.com (accessed November 1, 2022) (online, n.d.).
[61] FDA, Diclofenac 1% Gel: Prescribing Information, 2009.
[62] (European Agency for the Evaluation of Medicinal Products) EAEMP, Committee for Veterinary Medicinal Products. Diclofenac Summary Report. European Agency for the Evaluation of Medicinal Products Veterinary Medicines and Inspections. London, UK., Emea/Mrl/885/03-Final, 2003, pp. 1–9.